Article

Not peer-reviewed version

Synthesis and Characterization of Covalent Triazine Frameworks Based on 4,4‘-(Phenazine-5,10-diyl)dibenzonitrile and its Application in CO2/CH4 Separation

Hanibal Othman , Robert Oestreich , Vivian Küll , Markus N. A. Fetzer , Christoph Janiak *

Posted Date: 4 July 2025

doi: 10.20944/preprints202507.0335.v1

Keywords: covalent triazine frameworks; BET surface area; adsorption; carbon dioxide separation from methane; heat of adsorption

 doi:10.20944/preprints202507.0335.v1

Article

Synthesis and Characterization of Covalent Triazine Frameworks Based on 4,4'-(Phenazine-5,10-diyl) dibenzonitrile and its Application in CO_2/CH_4 Separation

Hanibal Othman, Robert Oestreich, Vivian Küll, Markus N. A. Fetzer and Christoph Janiak *

Institut für Anorganische Chemie und Strukturchemie, Heinrich-Heine-Universität Düsseldorf, 40204 Düsseldorf, Germany

* Correspondence: janiak@uni-duesseldorf.de

Abstract

Covalent triazine frameworks (CTFs) have gained recognition as stable porous organic polymers, for example, for CO_2 separation. From the monomer 4,4'-(phenazine-5,10-diyl)dibenzonitrile (pBN) new pBN-CTFs were synthesized using the ionothermal method with variation of temperature (400 and 550 °C) and $ZnCl_2$ to monomer ratio (10 and 20). N_2 adsorption yielded BET surface areas up to 1460 m^2g^{-1}. The pBN-CTFs are promising CO_2 adsorbents and are comparable to other benchmark CTFs such as CTF-1 with a CO_2 uptake of pBN-CTF-10-550 at 293 K of up to 54 $cm^3\ g^{-1}$ or 96 mg g^{-1}, having a CO_2/CH_4 IAST selectivity of 22 for a 50% mixture of CO_2/CH_4. pBN-CTF-10-400 has a very high heat of adsorption of 79 kJ mol^{-1} for CO_2 near zero coverage in comparison to other CTFs, which also stays well above heat of the liquefaction heat of CO_2 due to its high microporosity of 50% of the total pore volume.

Keywords: covalent triazine frameworks; BET surface area; adsorption; carbon dioxide separation from methane; heat of adsorption

1. Introduction

Porous materials contain interconnected pores which can have different length scales from micro- (< 2 nm), meso- (2–50) nm to macropores (>50 nm) [1,2]. Covalent triazine frameworks (CTFs) are micro-mesoporous organic polymers that are constructed from 1,3,5-triazine rings joined with linkers to ideally give two-dimensional networks with hexagonal openings (Figure 1) [3–5].

The nitrogen content and the porosity of the CTFs together with their thermal stability make them interesting materials for gas adsorption, storage and separation, pollutant removal, catalysis and sensing [6–13], including CO_2/N_2 and CO_2/CH_4 separation, both in the neat form [14–18] and as a filler for organic polymers in mixed-matrix membranes [19–21]. Since the inception of covalent triazine frameworks in 2008 [22], these materials were investigated for CO_2 adsorption [23–32].

One of the standard synthesis methods of CTFs is the ionothermal method, in which the nitrile monomer is heated with excess zinc chloride under vacuum or an inert atmosphere to a chosen temperature in the range between 400-900 °C [33]. In this reaction, the molten zinc chloride salt acts as a solvent, as a Lewis acid and as a porogen [34].

The surface area is not necessarily the determining and main property of CTFs for CO_2 adsorption. A study showed an inverse relation between BET surface area and the uptake of CO_2 [17]. This correlation can be understood by increase of the surface area with synthesis temperature and the concomitant decrease of the nitrogen content. When the CTFs are synthesized under relatively low temperatures (e.g., at 350 °C), the nitrogen loss is minimized but so is the surface area. Under higher synthesis temperatures (over 500 °C), significant nitrogen loss occurs, resulting in materials

 doi:10.20944/preprints202507.0335.v1

that transition towards high-surface area carbon structures with some residual nitrogen content. Often 400 °C is chosen as a compromise between good surface area and not too high nitrogen loss. For a high CO_2 uptake a high nitrogen content is aimed for [22].

In this work we use the dinitrile monomer 4,4'-(phenazine-5,10-diyl) dibenzonitrile (pBN) (Figure 1) to increase the nitrogen content for CO_2 adsorption and separation from CO_2/CH_4 mixtures. The CTFs from this monomer were synthesized with two ratios of $ZnCl_2$ to observe the impact of the salt ratio on the surface area and two temperatures to compare the effect of the temperature on the CO_2 and CH_4 adsorption.

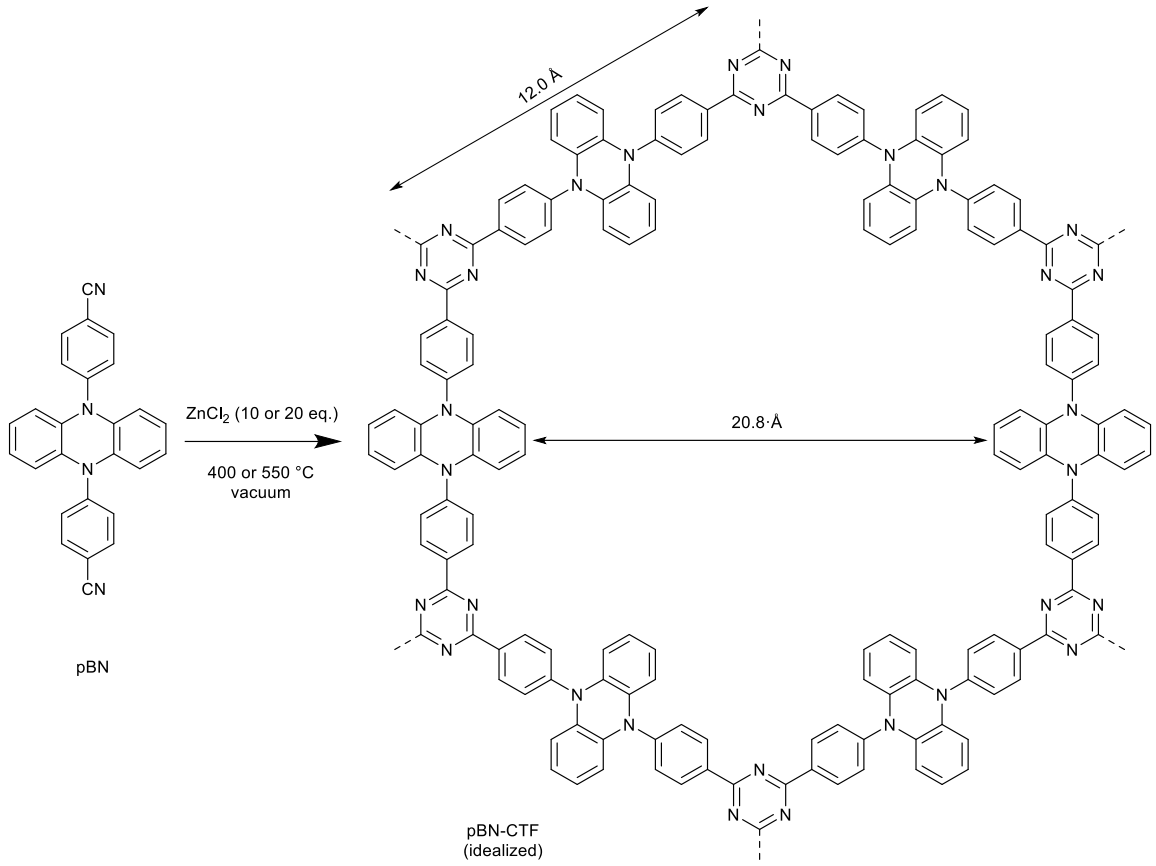

Figure 1. Synthesis of pBN-CTF from the monomer 4,4'-(phenazine-5,10-diyl)dibenzonitrile (pBN) with the CTF shown as idealized hexagonal ring structure. The edge length and width of the ideal hexagon were determined graphically on the basis of the length of the C=C double with 1.34 Å.

2. Results and Discussion

New covalent triazine frameworks with the monomer 4,4'-(phenazine-5,10-diyl)dibenzonitrile (pBN) were synthesized by the ionothermal route with molten zinc chloride at two molar $ZnCl_2$:monomer ratios of 10:1 and 20:1 at three temperatures of 350 °C, 400 °C and 550 °C, all at the reaction time of 48 h. The CTF samples are coded as pBN-CTF-xx-yyy by giving the molar $ZnCl_2$:monomer ratio (xx = 10 or 20), followed by the reaction temperature (yyy = 350, 400 or 550 °C). The pBN-CTF products were obtained as black monoliths, as typically observed for CTFs [35]. The $ZnCl_2$ was tried to be removed through washing with acidified water as described in the literature for CTFs [35,36]. Product yields ranged from 68-92% (Table 1). Scanning electron microscopy images indicate the typical shard-like morphology of CTFs (Figure S1a-d, Supplementary Material).

 doi:10.20944/preprints202507.0335.v1

Table 1. Summary of the reaction parameters and yields for pBN-CTFs.

CTF product [a]	Molar ratio $ZnCl_2$:monomer	Temperature (°C)	Yield (%)
pBN-CTF-10-350	10	350	79
pBN-CTF-20-350	20	350	78
pBN-CTF-10-400	10	400	68
pBN-CTF-20-400	20	400	92
pBN-CTF-10-550	10	550	84
pBN-CTF-20-550	20	550	40

[a] The first number in the product name after CTF gives the molar $ZnCl_2$:monomer ratio (10 or 20), followed by the reaction temperature (400 or 550 °C).

In the infrared spectra the characteristic C-N stretching band of the triazine units was observed at 1384 and 1508 cm^{-1} slightly shifted from the C-N breathing and stretching mode of a molecular triazine unit (1363 and 1511 cm^{-1}, respectively), in agreement with the infrared spectra of other CTFs [37,38]. At the same time the CN band of the monomer at 2227 cm^{-1} has disappeared (Figure S2, Supplementary Material), signaling that the monomer was consumed during the polymerization.

The CHN elemental combustion analysis reveals the typical nitrogen loss which increases with higher temperature (Table S1). The nitrogen loss is due to a partial aromatic nitrile decomposition into HCN, CN radicals, NH_3 and other species from the synthesis at the temperature of several hundred °C [3,5,36,40–46]. It can be seen that the C/N ratio is increased while the C/H ratio does not change much and stays close to the theoretical ratio, thereby indicating the primary loss of nitrogen-rich species. These results correlate with the general observation that an increase in temperature in ionothermal CTF synthesis leads to enhanced carbonization of the samples [5,12,40,43]. To avoid the nitrogen loss, we have also performed the pBN-CTF formation at 350 °C. It became evident, however, that the surface area, porosity and gas sorption of the samples at 350 °C varied greatly from batch to batch and among different probes from the same batch (Section S4, Figure S5, Figure S6, Table S2). Thus, samples at 350 °C were inhomogeneous and could not be reproducibly synthesized. Therefore, results from the reaction temperature at 350 °C were not included in the discussion here in the main text.

The remaining difference of the combined weight percentage of C, H and N to 100% amounts to ~20% and is usually explained by residual $ZnCl_2$ or by the adsorption of water upon sample handling. Energy-dispersive X-ray spectroscopy (EDX) gave a consistent amount of both Zn (~4.5 wt%) and Cl (7-10 wt%, Table S1). The $ZnCl_2$ which is embedded in the pores of the CTFs is difficult to remove even by extended washing, as some of the pores may no longer be accessible. The still remaining difference of ~5 wt% was shown to be due to the adsorption of moisture from air in the porous CTF. We have recently verified that CTFs are hygroscopic, with a water uptake of up to 0.12–0.20 g g^{-1} (equivalent to 11–17 wt%) at 50–60% air humidity (that is $P/P_0 \approx 0.5–0.6$) when handled or stored under ambient air [15,43,47].

Powder X-ray diffractograms (PXRDs) yield only broad reflexes without any clear signature of (001) reflections for parallel two-dimensional sheets in eclipsed stacking (Figure S3), which indicates a very amorphous structure because of defects in the idealized hexagonal sheets with possibly partial interpenetration or three-dimensional framework arrangements.

The nitrogen sorption isotherms of the CTFs in Figure 2 show all a pronounced adsorption step at $P/P_0 < 0.05$ corresponding to gas sorption in micropores (pores < 2nm, Figure 3, see Figure S5a for the 350 °C samples). The adsorption isotherms at 400 °C are largely of Type Ib, indicative of materials with micropore size distributions over a broader range and narrow mesopores (pores > 2 nm, Figure 3a,b, Table 2) [1]. There is a H4 hysteresis, where the hysteresis loop closes only at very low relative pressure P/P_0. Such H4 loops are found among others with micro-mesoporous carbons [1,2]. For 550 °C, the adsorption isotherm of the 10-550 sample appears to be a Type I and IV combination. The adsorption branch has a "knee" at P/P_0 ~0.4 and the saturation plateau, which is a typical feature of

 doi:10.20944/preprints202507.0335.v1

Type IV isotherms, is then reached at high P/P_0. Type IV isotherms are given by largely mesoporous adsorbents (Figure 3c,d, Table 2). The isotherm at 550 °C has a hysteresis loop of Type H2b which is associated with pore blocking in a wide range of pore neck widths. The N_2 adsorption isotherm of the sample 20-550 can be assigned as a mixture of Type I and Type II isotherms. The nitrogen uptake does not saturate towards $P/P_0 = 1$ which is due to a Type II branch. Type II indicates macropores (pores > 50 nm) which can also be caused by the voids between the particles. The isotherm has a H3 hysteresis loop that correlate with macropores that are not filled with pore condensate [1,2].

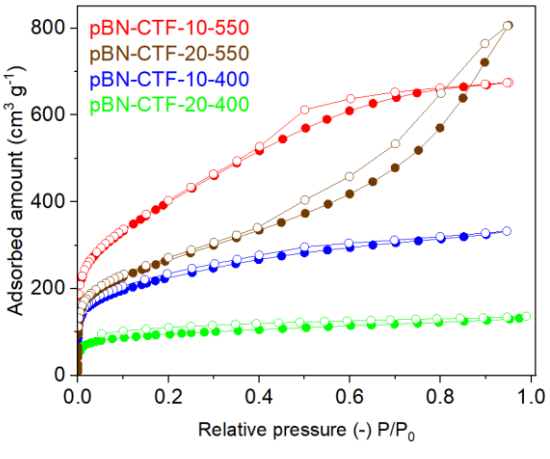

Figure 2. N_2 isotherms (at 77 K) of pBN-CTFs (filled symbols adsorption, empty symbols desorption).

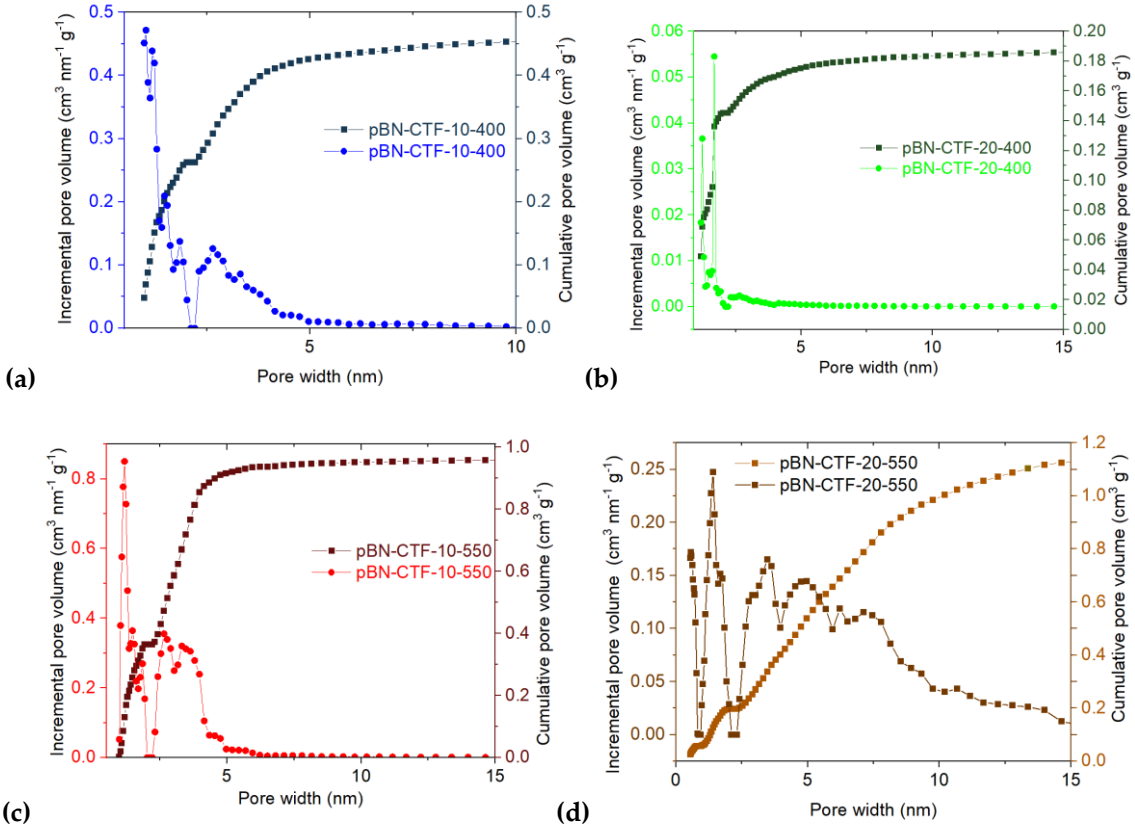

Figure 3. (**a**)-(**d**) NLDFT pore size distribution (PSD) curves showing the cumulative pore volume (right y axes) and the incremental pore volume (left y axes) of pBN-CTF from N_2 adsorption using the "N_2 at 77 K on carbon slit-pore, NLDFT equilibrium model".

The specific surface areas were obtained from the Brunauer–Emmett–Teller (BET) model over the pressure range of $P/P_0 \approx 0.01$-0.07. Generally, the surface areas are higher for the 10:1 than for the

 doi:10.20944/preprints202507.0335.v1

20:1 $ZnCl_2$: monomer ratios, giving 809-1460 $m^2\ g^{-1}$ for the former and only 348-950 $m^2\ g^{-1}$ for the latter (Table 2).

Table 2. Surface area and porosity data from N_2 and CO_2 sorption studies.

CTF Product	S_{BET} [a] ($m^2\ g^{-1}$)	V_{tot} [b] ($cm^3\ g^{-1}$)	V_{micro} [c] ($cm^3\ g^{-1}$)	V_{micro}/V_{tot} [d]	$V_{1nm}(CO_2)$ [e] ($cm^3\ g^{-1}$)
pBN-CTF-10-400	809	0.51	0.25	0.50	0.015
pBN-CTF-20-400	348	0.19	0.15	0.79	0.009
pBN-CTF-10-550	1460	1.04	0.36	0.35	0.013
pBN-CTF-20-550	950	1.25	0.19	0.31	0.010

[a] Calculated BET surface area from N_2 adsorption at 77 K over a pressure range of P/P_0 = 0.01-0.07; [b] Total pore volume from N_2 adsorption isotherm at 77 K at P/P_0 =0.95 for pores smaller than 40 nm; [c] Micropore volume from the NL-DFT method using the N_2 adsorption isotherm at 77 K at P/P_0 = 0.1 for pores with d ≤ 2 nm (20 Å). [d] Micropore volume/total pore volume. [e] Pore volume for pores with diameters smaller than 1 nm from CO_2 adsorption isotherms at 293 K and the CO_2 NL-DFT model.

In other CTF synthesis, e.g., with the tetra(4-cyanophenyl)ethylene monomer $ZnCl_2$:monomer ratios of 10:1 and 20:1 were compared, with the former giving a more than two-fold higher surface area (2235 vs. 784 $m^2\ g^{-1}$) [48,49]. Thus, a ratio of 10:1 seems optimal for many ionothermal CTF syntheses. In the following, we will therefore only discuss the results for the 10:1 molar ratio, that is, the pBN-CTF-10 series. In agreement with other CTF works, the surface area of the sample synthesized at 400 °C is lower than that at 550 °C (Table 2, Figure 2) as generally the surface areas and total pore volumes for the resulting products increase with temperature [43]. The surface areas of the pBN-CTFs are comparable with other CTFs with longer linkers, e.g., terphenyl prepared by Kuhn et al. with a surface area of 975 $m^2\ g^{-1}$ [22], or even 2,8-dicyano-6H,12H-5,11-methanodibenzo[1,5] diazocine that was synthesized by Wang et al. with 612 $m^2\ g^{-1}$ [50].

Using NL-DFT calculations with a slit-pore model on the N_2 adsorption isotherms, the pore widths and distribution as well as the total and micropore volume can be estimated (Figure 3, Figure S5, Table 2) [36]. The pore width distribution diagrams for the CTF-400s indicate pronounced maxima in the micropore region (<2 nm) and pore sizes larger than 2 nm in a broad distribution. At 400 °C, the micropore volume encompasses more than 50% of the total pore volume, that is V_{micro}/V_{tot} values are above 0.50, (Table 2). At 550 °C the total pore volume more than doubles in comparison to 400 °C and pore width distributions exhibit more p broader contribution of mesopores between 2 and ~5 nm (Figure 3c) and beyond (Figure 3d), such that V_{micro}/V_{tot} drops below 35% (Table 1). Noteworthy, the material with the highest surface area pBN-CTF-10-550 has the lowest micropore volume fraction V_{micro}/V_{tot}.

The pore size distribution (PSD) from N_2 sorption at 77 K is generally limited to pores between ~1 to ~40 nm. Macropores (> 50 nm) are not accounted anymore by N_2 sorption. For pores smaller than 1 nm (10 Å), the size and distribution need to be obtained from CO_2 gas adsorption data, because for N_2 sorption at 77 K the diffusion of the molecules into micropores smaller than 1 nm is very slow, hence would require very long N_2 adsorption measurements for equilibration of the adsorption isotherms, which cannot be assured. To avoid erroneous PSD results from the N_2 adsorption analysis, CO_2 adsorption analysis can be used (Figure 4a,b). The saturation pressure of CO_2 at 10 °C is ~4480 kPa (~33450 Torr), so that a low relative pressure which is necessary for the micropore analysis is achieved in the range of moderate absolute pressures [51]. The micropore analysis with CO_2 at 283 K instead of N_2 at 77 K allows for a faster equilibration and access of even smaller pores as the kinetic diameter of CO_2 is only 3.30 Å versus 3.64 Å for N_2. The NL-DFT analysis of the CO_2 adsorption isotherms of the pBN-CTF-10s with the "CO_2 on carbon based slit-pore" model yield similar corrugated pore size distribution curves for the CTFs below 1 nm with pronounced maxima between 0.5-0.9 nm and at ~0.85 nm (Figure 2). The surface area was also calculated using the CO_2 adsorption at 195 K (values can be seen in Table 3 and isotherms in Figure S6) which gave a smaller surface area

 doi:10.20944/preprints202507.0335.v1

that that of the N_2 counterpart, corresponding to Literature where similar material was investigated [48,52–55].

Volumetric CO_2 and CH_4 adsorption studies resulted in the isotherms depicted in Figure 4. At 283 K and 293 K the pBN-CTF-10 materials show similar CO_2 sorption isotherm curvatures which did not level off much at 1 bar but still have rather positive slope which indicates the uptake at 1 bar is far from saturation. At 195 K the CO_2 uptake at 1 bar differentiates considerably for the pBN-CTF-10-400 and 10-550 material (Table 3, Figure S7), increasing nearly two-fold from pBN-CTF-10-400 with 175 $cm^3\ g^{-1}$ to pBN-CTF-10-550 with 320 $cm^3\ g^{-1}$. This increase correlates with the increase in surface area and pore volume from the 400 °C to the 550 °C material in Table 2.

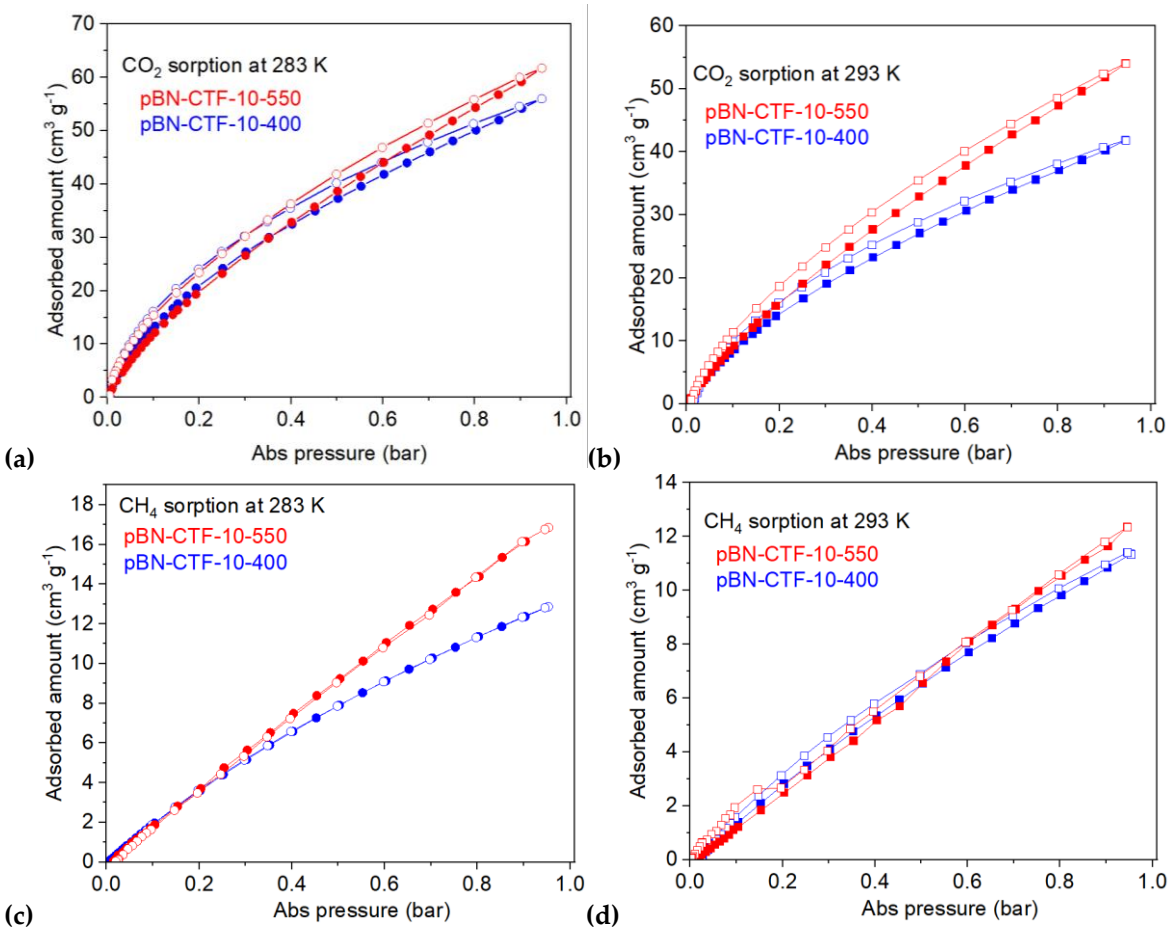

Figure 4. Adsorption and desorption isotherms of CTF-10s for (a) CO_2 at 283 K, (b) CO_2 at 293 K, (c) CH_4 at 283 K and (d) CH_4 at 293 K (filled symbols adsorption, empty symbols desorption). The CO_2 adsorption isotherms at 195 K are given in Figure S7, for the CTF-20s at 293 K in Figure S8.

Table 3. CO_2 and CH_4 adsorption results at 1 bar, heat of adsorption for CO_2 at zero coverage and CO_2:CH_4 selectivity.

CTF product	S_{BET} (195 K) [a] ($m^2\ g^{-1}$)	CO_2 ($cm^3\ g^{-1}$)			CH_4 ($cm^3\ g^{-1}$)		CO_2 $Q_{ads}{}^0$ [b] (kJ mol^{-1})	CH_4 $Q_{ads}{}^0$ [b] (kJ mol^{-1})	IAST selectivity for 50:50 CO_2:CH_4
		293 K	283 K	195 K	293 K	283 K			
pBN-CTF-10-400	524	42.8	55.9	175	11.3	12.9	79	36	22
pBN-CTF-10-550	746	54.0	61.7	320	12.3	16.9	60	39	-[c]

[a] BET surface area from CO_2 adsorption measured at 195 K in the range between 0.08 and 0.2 P/P_0. The difference in surface area between N_2 (77 K) and CO_2 (195 K) can be due to the kinetic energy difference at different temperature and also the size of the molecules adsorbed. [b] Isosteric heat of adsorption of CO_2 or CH_4 towards zero loadings from the adsorption isotherms at 283 K and 293 K. [c] IAST selectivity for 50:50 mol:mol or

 doi:10.20944/preprints202507.0335.v1

equimolar fraction of CO_2 and CH_4 at 293 K and 1 bar. The linear CH_4 uptake of CTF-10-550 did not allow for a meaningful fit.

Comparing the pBN-CTFs from this work to other CTFs with linkers equal or longer than a biphenyl unit it can be seen that the pBN-CTFs can compete very well in terms of CO_2 uptake (Figure 5, Table S4).

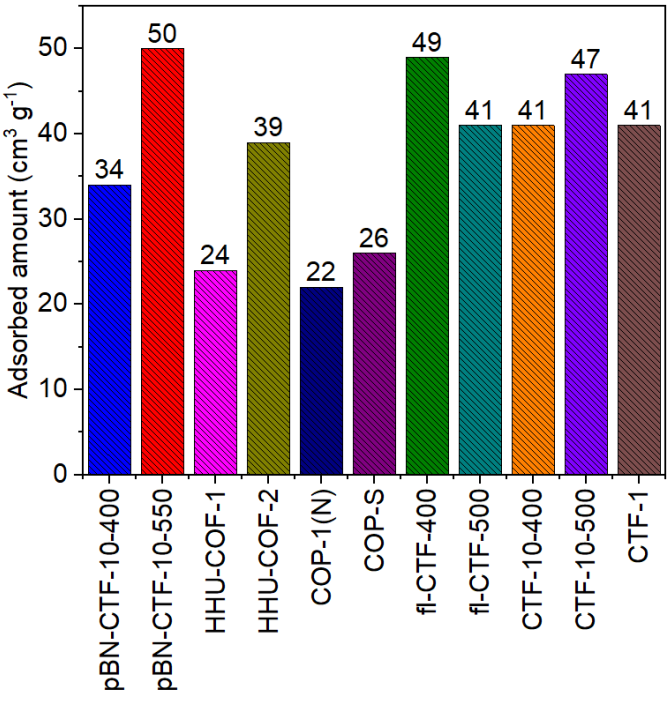

Figure 5. CO_2 uptake comparison at 298 K and 1 bar between the pBN-CTFs and selected CTFs with data from Table S4 [18,53,59,62,64,65]. The CTFs all have a linker with a length of at least a biphenyl unit, except for the reference of prototypical CTF-1.

Covalent triazine frameworks are widely investigated for CO_2/N_2 and CO_2/CH_4 separation. The ideal adsorbed solution theory (IAST) can give an indication of the selectivity in different gas mixtures at a given pressure or for a given gas mixture at different pressures. The only criterion that IAST requires is that both gases should have an equal spreading pressure at the given temperature [56]. The IAST selectivity is derived from the single gas adsorption isotherms and was calculated here on the bases of fitting the adsorption isotherms with the Freundlich-Langmuir adsorption model and the parameters that resulted from the isotherm fitting (Table S5) were used in calculating the selectivity (Table 3).

IAST underscores the selectivity for CO_2 over CH_4 for the pBN-CTF-10-400 material, as seen already in the higher uptake of CO_2 over CH_4 at the same temperature (Table 3). At 283 K the slightly pressure and composition dependent CO_2/CH_4 selectivity for pBN-CTF-10-440 varies between 7-22. It decreases with pressure and increases with increasing CH_4 fraction (Figure S11). At 293 K the CO_2/CH_4 selectivity for pBN-CTF-10-440 stays rather constant between 0.01-0.8 CH_4 molar fraction. The preference for CO_2 can be explained from the pore structure and the interaction strength between the gas molecules and the framework. pBN-CTF-10-400 has a good microporosity and nitrogen content. Micropores favor CO_2 adsorption due to its smaller kinetic diameter (3.3 Å) compared to CH_4 (3.8 Å), while nitrogen functionalities enhance CO_2 affinity through dipole-quadrupole interactions.

From a measurement of gas adsorption at two temperatures with ΔT = 10 to 20 °C the enthalpy (ΔH) or heat of gas adsorption ($Q_{ads} = -\Delta H$) can be obtained [13,57]. Near zero coverage the heat of adsorption for CO_2 is remarkably high in comparison to other CTFs with 79 kJ mol^{-1} for pBN-CTF-

 doi:10.20944/preprints202507.0335.v1

10-400 (Table S6). In Figure 6 the isosteric heat of adsorption was plotted against the amount of CO_2 and CH_4 adsorbed by the frameworks. pBN-CTF-10-400 has a higher microporosity and higher nitrogen content than pBN-CTF-10-550. This relates to a higher affinity for CO_2 than for CH_4 because (as just noted) CO_2 with its smaller kinetic diameter (3.3 Å) compared to CH_4 (3.8 Å) can occupy smaller micropores, and the CO_2 quadrupole can interact with the dipole of nitrogen functionalities. Micropores generally allow for multi-site or "wall···guest···wall" interactions between guest molecules and the inner pore surface. The large decrease in the isosteric heat of adsorption from near zero adsorbed amount to ~0.5 mmol g^{-1} adsorbed amount seen in Figure 6 for both gases is due to the initial filling of the very small or ultra-micropores with a diameter in the dimension of the adsorbate molecule with wall-to-wall interactions and the occupation of the nitrogen atom sites which also have higher adsorption energies. Noteworthy, the CO_2 heat of adsorption values of pBN-CTF-10-550 drop below the liquefaction heat of CO_2 of 17 kJ mol^{-1} when the adsorbed amount surpasses 1.1 mmol g^{-1} while the heat of adsorption of pBN-CTF-10-400 stays well above the liquefaction heat of CO_2.

Conversely, pBN-CTF-10-550 exhibits a higher Q_{ads} for CH_4 over the whole uptake range compared to pBN-CTF-10-400 and also a higher heat of adsorption for CH_4 than for CO_2 once the adsorbed CO_2 amount exceeded ~0.4 mmol g^{-1} (compare Figure 6a and b). This can be explained by the more carbon-like non-polar nature of the pBN-CTF-10-550 material with less nitrogen content than pBN-CTF-10-400 which gives the former a relatively higher affinitiy to non-polar CH_4. As expected, the heat of adsorption near zero coverage is lower for CH_4 than for CO_2 for both CTFs (Table 3). Further literature comparison for CO_2 uptake and Q_{ads}^0 for CO_2 in CTFs can be found in Table S4 and Table S6, respectively, in the Supplementary Material [15,19,26,27,59–72].

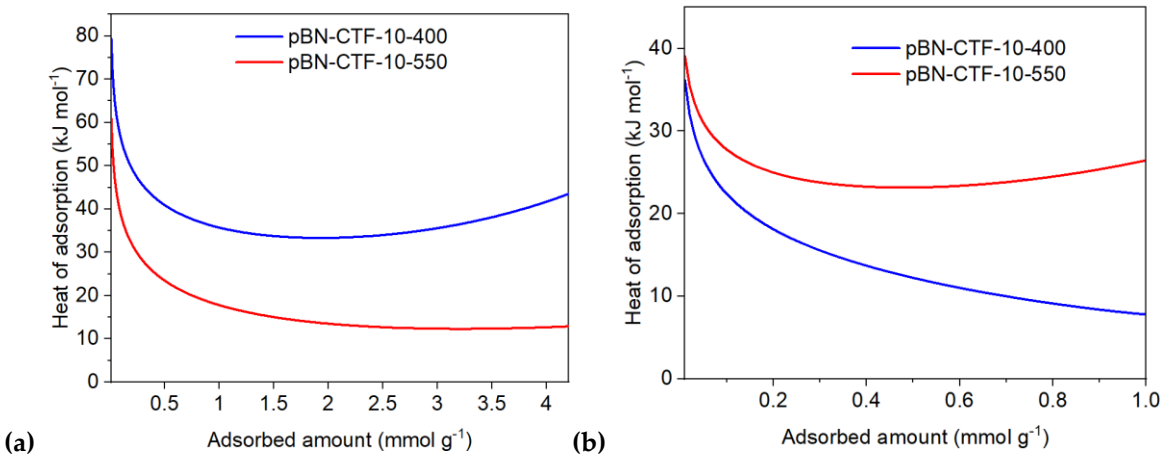

Figure 6. Isosteric heat of adsorption for (**a**) CO_2 and (**b**) CH_4 on pBN-CTF-10-400 and 550.

Thermogravimetric analysis showed that under air all samples started decomposing (with weight loss) at ~400 °C, including the pBN-CTF which was synthesized at 550 °C (Figure S13). This mass loss of the pBN-CTF-10-400 sample is complete below 700 °C with a residual mass of ~2.5 wt%. The mass loss of the pBN-CTF-10-550 continues to ~770 °C, leaving only ~0.2 wt%.

3. Conclusions

The molecule 4,4'-(phenazine-5,10-diyl)dibenzonitrile with a long about 12 Å separation between the nitrile groups can be successfully transformed by ionothermal synthesis into a porous covalent triazine framework (pBN-CTF). The surface area increases expectedly with the synthesis temperature and ranges from 809 to 1460 m^2 g^{-1} for the samples synthesized at 400 and 550 °C, respectively, with pores ranging between 1-4 nm. The pBN-CTF exhibited a good CO_2 uptake at 293 K, having a similar performance as benchmark materials like CTF-1, due to the relatively high micropore fraction that ranged between 35% for the 550 °C and 50% for the 400 ° samples. The new material showed significant difference and stark contrast in the adsorption of CO_2 over CH_4 for the

 doi:10.20944/preprints202507.0335.v1

potential separation with a selectivity that reaches 22. For further work on pBN-CTFs and other CTFs in general we plan to increase the nitrogen content of the formed framework through the addition of a nitrogen-rich compound such as melamine in order to introduce additional electron pair donors and, thereby, influence the adsorption properties. We will also check into the elongation of the phenyl group in pBN with a biphenyl group, giving the monomer 4',4'''-(phenazine-5,10-diyl)bis(([1,1'-biphenyl]-4-carbonitrile)).

4. Materials and Methods

4.1. Instrumentation

Fourier transform infrared spectroscopic measurements were done using a Bruker Tensor 37 (Bruker AXS, Karlsruhe, Germany) with KBr pellets in the range between 4000-500 cm^{-1}. For the N_2 sorption analysis a Quantachrome Autosorb-IQ-MP (Quantachrome, Boynton Beach, FL, USA) was used. The samples were degassed for 24 h at 120 °C before connecting to the device. The measurement was done at 77 K. The results were interpreted with the BET equation. The CO_2 sorption analysis was done with a Quantachrome Autosorb-IQ-MP (Quantachrome, Boynton Beach, FL, USA). The measurement temperature was 293, 283 and 195 K after activating (degassing) the samples under vacuum at 120 °C for 24 h. The temperature was held by virtue of a thermostated water bath (293 and 283 K) or with a cryodyne refrigerator model 8200 (195 K) (Janis, Woburn, Massachusetts, USA).

Thermogravimetric analysis was performed with a TG Tarsus 209 F3 (Netzsch, Selb, Germany). The samples were analyzed under synthetic air with a heating rate of 10 K/min from 25-900 °C. Powder X-ray diffraction patterns were recorded using a Bruker D2 phaser from Bruker (Bruker AXS, Karlsruhe, Germany) with Cu-Kα radiation, λ = 1.54182 Å at 300 W, 30 kV, 10 mA. Nuclear magnetic resonance (^{1}H-NMR) spectra were collected with a Bruker Avance III-600-I (Bruker, Karlsruhe, Germany). The chemical shifts are given in ppm and are referenced to the residual proton signal of the deuterated solvent (7.26 ppm for $CDCl_3$, 7.16 for C_6D_6).

4.2. Chemicals

Phenazine (99.86%) and 4-bromobenzonitrile (95%) was obtained from BLDpharm. Sodium dithionite (85%) was obtained from VWR chemicals. Palladium acetate (99.9%) and tri-tert-butyl phosphine (99%) was bought from Aldrich. All solvents were purchased from commercial suppliers with a minimum purity of 99.8%.

4.3. Synthesis of 5,10-dihydrophenazine

Following the literature [58] a phenazine (2.5 g, 13.87 mmol) solution in ethanol (30 mL) and a sodium dithionite (24.1 g, 137 mmol) solution in water (125 mL) are placed into a round-bottom flask and heated to reflux at 95 °C for 3 hours- Afterwards the flask was cooled to room temperature, the product is separated by filtration, washed three times with water (3 x 15mL), dried under vacuum (10^{-3} mbar) and stored under nitrogen to avoid any oxidation. Yield 2.10 g, 85%.

^{1}H NMR (600 MHz, $CDCl_3$) δ 8.27 (dd, *J* = 6.8, 3.5 Hz, 1H), 7.86 (dd, *J* = 6.8, 3.4 Hz, 1H), 6.12 (s, 2H), 1.57 (s, 3H).

4.4. Synthesis of 4,4'-(phenazine-5,10-diyl)dibenzonitrile (pBN)

5,10-Dihydrophenazine (2 g, 11 mmol), 4-bromobenzonitrile (4.38 g, 24 mmol), and potassium carbonate (9.1 g, 65.8 mmol) are combined in degassed toluene (80 mL) in a round-bottom flask under N_2 atmosphere according to the literature [56]. To this mixture, palladium acetate (0.141 g, 0.62 mmol) and tri-tert-butyl phosphine (0.464 g, 2.30 mmol) dissolved in 10 mL toluene are added, the flask is then refluxed at 111 °C for 20 h. During cooling, water (30 mL) was added to the reaction mixture in order to stop the reaction. The product was extracted from the water phase using chloroform (200 mL). The separated organic phase was washed with brine (saturated aqueous NaCl solution) three

 doi:10.20944/preprints202507.0335.v1

times (3 x 30 mL) and was dried over magnesium sulphate ($MgSO_4$) for 15 min. The organic phase was then filtered and concentrated via a rotary evaporator to ~50 mL, after that 100 mL of n-hexane was added and cooled in an ice bath for 10 min. The separated product was filtered and dried in a vacuum (10^{-3} mbar) at 60 °C.

^{1}H NMR (600 MHz, C_6D_6) δ 6.96 (d, *J* = 8.2 Hz, 4H), 6.71 (d, *J* = 8.2 Hz, 4H), 6.41 – 6.37 (m, 4H), 5.69 (dt, *J* = 7.9, 3.9 Hz, 4H).

4.5. pBN-CTF synthesis:

Inside the glove box a glass ampule with a Schlenk fitting was filled with (0.2 g, 0.5 mmol) pBN-2CN and 10 or 20 equivalents (0.680 g, 5 mmol or 1.3 g, 10 mmol) of anhydrous zinc chloride. Outside the glovebox, the ampule was evacuated and flame sealed and heated for 48 h in a tube furnace at the chosen temperature of 350, 400 or 550 °C. The 350 and 400 °C reactions were done in a normal borosilicate glass (Pyrex), for 550 °C a quartz glass ampule was used. After cooling the ampule to room temperature, the ampule was carefully opened with no sign of pressure built-up inside.

The reaction product was stirred in distilled water acidified with 0.5 mol/L hydrochloric acid (HCl) to pH = 4 (50 mL) for three days. The stirring was done vigorously to ensure the mechanical break-up of the black monolith to give fine particles. After additional stirring for 72 h in distilled water, the product is filtered and washed with the organic solvents chloroform, acetone, and methanol (30 mL each) in this order. After the washings, the product was dried in a vacuum (10^{-3} mbar) oven at 60 °C for 24 h. Yields are listed in Table 1.

Supplementary Materials: The following supporting information can be downloaded at the website of this paper posted on Preprints.org, Section S1. Scanning electron microscopy; S2. Fourier transform infrared spectroscopy and elemental analysis; Section S3. Powder X-ray diffraction; Section S4. Samples synthesized at 350 °C and their N_2 and CO_2 sorption studies; Section S5. CO_2 adsorption isotherms; Section S6. Calculations and fitting for the isosteric heat of adsorption and IAST selectivity of CO_2 and CH_4; Section S7. Thermogravimetric analysis (TGA), Section S8. Nuclear magnetic resonance spectrometry (NMR); Section S9. References.

Author Contributions: Conceptualization, H.O.; methodology, H.O., V.K., R.O. and M.F.; software, H.O.; validation, C.J and H.O.; formal analysis, H.O.; investigation, H.O.; resources, C.J.; data curation, H.O.; writing—original draft preparation, H.O.; writing—review and editing, H.O. and C.J.; visualization, H.O.; supervision, C.J.; project administration, C.J. All authors have read and agreed to the published version of the manuscript.

Funding: This research received no external funding.

Data Availability Statement: The original contributions presented in this study are included in the article/supplementary material. Further inquiries can be directed to the corresponding author(s).

Acknowledgments: Special thanks goes to Dietrich Püschel for his advice and supervision and to Birgit Tommes for her IR measurements.

Conflicts of Interest: The authors declare no conflict of interest.

References

1. Thommes, M.; Kaneko, K.; Neimark, A.V.; Olivier, J.P.; Rodriguez-Reinoso, F.; Rouquerol, J.; Sing, K.S.W. Physisorption of gases, with special reference to the evaluation of surface area and pore size distribution (IUPAC Technical Report). *Pure Appl. Chem*. **2015**, *87*, 1051-1069. doi:10.1515/pac-2014-1117.
2. Cychosz, K.A.; Thommes, M. Progress in the Physisorption Characterization of Nanoporous Gas Storage Materials. *Engineering* **2018**, *4*, 559-566. https://doi.org/10.1016/j.eng.2018.06.001.
3. Bojdys, M.J.; Jeromenok, J.; Thomas, A.; Antonietti, M. Rational Extension of the Family of Layered, Covalent, Triazine-Based Frameworks with Regular Porosity. *Adv. Mater*. **2010**, *22*, 2202-2205. https://doi.org/10.1002/adma.200903436.

 doi:10.20944/preprints202507.0335.v1

4. Meier, C.B.; Clowes, R.; Berardo, **B**E.; Jelfs, K.E.; Zwijnenburg, M.A.; Sprick, R.S.; Cooper, A.I. Structurally Diverse Covalent Triazine-Based Framework Materials for Photocatalytic Hydrogen Evolution from Water. *Chem. Mater*. **2019**, *31*, 8830-8838. doi:10.1021/acs.chemmater.9b02825.
5. Kuhn, P.; Forget, A.; Su, D.; Thomas, A.; Antonietti, M. From Microporous Regular Frameworks to Mesoporous Materials with Ultrahigh Surface Area: Dynamic Reorganization of Porous Polymer Networks. *J Am. Chem. Soc*. **2008**, *130*, 13333-13337. doi:10.1021/ja803708s.
6. Kuecken, S.; Acharjya, A.; Zhi, L.; Schwarze, M.; Schomäcker, R.; Thomas, A. Fast tuning of covalent triazine frameworks for photocatalytic hydrogen evolution. *Chem. Commun*. **2017**, *53*, 5854-5857, doi:10.1039/C7CC01827D.
7. Liao, L.; Li, M.; Yin, Y.; Chen, J.; Zhong, Q.; Du, R.; Liu, S.; He, Y.; Fu, W.; Zeng, F. Advances in the Synthesis of Covalent Triazine Frameworks. *ACS omega* **2023**, *8*, 4527-4542. https://doi.org/10.1021/acsomega.2c06961
8. Liu, M.; Guo, L.; Jin, S.; Tan, B. Covalent triazine frameworks: synthesis and applications. *J. Mater. Chem. A* **2019**, *7*, 5153-5172. https://doi.org/10.1039/C8TA12442F
9. Lee, J.-S.M.; Cooper, A.I. Advances in Conjugated Microporous Polymers. *Chem. Rev.* **2020**, *120*, 2171–2214. https://doi.org/10.1021/acs.chemrev.9b00399
10. Krishnaraj, C.; Jena, H.S.; Leus, K.; van der Voort, P. Covalent triazine frameworks – a sustainable perspective. *Green Chem.* **2020**, *22*, 1038–1071. https://doi.org/10.1039/C9GC03482J
11. Aggarwal, S.; Awasthi, S.K. Emerging trends in the development and applications of triazine-based covalent organic polymers: a comprehensive review. *Dalton Trans.* **2024**, *53*, 11601–11643. https://doi.org/10.1039/D4DT01127A
12. Bhunia, A.; Esquivel, D.; Dey, S.; Fernández-Terán, R.; Goto, Y.; Inagaki, S.; Van Der Voort, P.; Janiak, C. A photoluminescent covalent triazine framework: CO_2 adsorption, light-driven hydrogen evolution and sensing of nitroaromatics. *J. Mater. Chem. A* **2016**, *4*, 13450-13457. http://dx.doi.org/10.1039/c6ta04623a
13. Gao, Q.; Li, X.; Ning, G.-H.; Leng, K.; Tian, B.; Liu, C.; Tang, W.; Xu, H.-S.; Loh, K.P. Highly photoluminescent two-dimensional imine-based covalent organic frameworks for chemical sensing. *Chem. Commun*. **2018**, *54*, 2349-2352. doi:10.1039/C7CC09866A
14. Bhunia, A.; Dey, S.; Bous, M.; Zhang, C.; von Rybinski, W.; Janiak, C. High adsorptive properties of covalent triazine-based frameworks (CTFs) for surfactants from aqueous solution. *Chem. Commun*. **2015**, *51*, 484-486. doi:10.1039/C4CC06393G.
15. Dey, S.; Bhunia, A.; Esquivel, D.; Janiak, C. Covalent triazine-based frameworks (CTFs) from triptycene and fluorene motifs for CO_2 adsorption. *J. Mater. Chem. A* **2016**, *4*, 6259-6263. doi:10.1039/C6TA00638H.
16. Wessely, I.D.; Schade, A.M.; Dey, S.; Bhunia, A.; Nuhnen, A.; Janiak, C.; Bräse, S. Covalent Triazine Frameworks Based on the First Pseudo-Octahedral Hexanitrile Monomer via Nitrile Trimerization: Synthesis, Porosity, and CO_2 Gas Sorption Properties. *Materials* **2021**, *14*, 3214. https://doi.org/10.3390/ma14123214.
17. Wang, K.; Huang, H.; Liu, D.; Wang, C.; Li, J.; Zhong, C. Covalent Triazine-Based Frameworks with Ultramicropores and High Nitrogen Contents for Highly Selective CO_2 Capture. *Environ. Sci. Technol.* **2016**, *50*, 4869-4876. doi:10.1021/acs.est.6b00425.
18. Bügel, S.; Hähnel, M.; Kunde, T.; de Sousa Amadeu, N.; Sun, Y.; Spieß, A.; Beglau, T.H.Y.; Schmidt, B.M.; Janiak, C. Synthesis and Characterization of a Crystalline Imine-Based Covalent Organic Framework with Triazine Node and Biphenyl Linker and Its Fluorinated Derivate for CO_2/CH_4 Separation. *Materials* **2022**, *15*(8), 2807. https://doi.org/10.3390/ma15082807.
19. Dey, S.; Bügel, S.; Sorribas, S.; Nuhnen, A.; Bhunia, A.; Coronas, J.; Janiak, C. Synthesis and Characterization of Covalent Triazine Framework CTF-1@Polysulfone Mixed Matrix Membranes and Their Gas Separation Studies. *Front. Chem*. **2019**, *7*, doi:10.3389/fchem.2019.00693.
20. Bügel, S.; Spieß, A.; Janiak, C. Covalent triazine framework CTF-fluorene as porous filler material in mixed matrix membranes for CO_2/CH_4 separation. *Microporous Mesoporous Mater*. **2021**, *316*, 110941, https://doi.org/10.1016/j.micromeso.2021.110941.
21. Bügel, S.; Hoang, Q.-D.; Spieß, A.; Sun, Y.; Xing, S.; Janiak, C. Biphenyl-Based Covalent Triazine Framework/Matrimid® Mixed-Matrix Membranes for CO_2/CH_4 Separation. *Membranes* **2021**, *11*, 795. https://doi.org/10.3390/membranes11100795. .

 doi:10.20944/preprints202507.0335.v1

22. Kuhn, P.; Antonietti, M.; Thomas, A. Porous, Covalent Triazine-Based Frameworks Prepared by Ionothermal Synthesis. *Angew. Chem. Int. Ed*. **2008**, *47*, 3450-3453. https://doi.org/10.1002/anie.200705710.
23. Buyukcakir, O.; Je, S.H.; Talapaneni, S.N.; Kim, D.; Coskun, A. Charged Covalent Triazine Frameworks for CO_2 Capture and Conversion. *ACS App Mater Interfaces*. **2017**, *9*, 7209-7216. doi:10.1021/acsami.6b16769.
24. Gu, C.; Liu, D.; Huang, W.; Liu, J.; Yang, R. Synthesis of covalent triazine-based frameworks with high CO_2 adsorption and selectivity. *Polym. Chem*. **2015**, *6*, 7410-7417, doi:10.1039/C5PY01090J.
25. Mukhtar, A.; Mellon, N.B.; Bustam, M.A.; Saqib, S.; Lee, S.-P.; Kareem, F.A.A.; Ullah, S. Impact of amine functionality on the selective CO_2/CH_4 adsorption behavior of porous covalent triazine adsorbent. *J. Nat. Gas Eng*. **2020**, *83*, 103582, https://doi.org/10.1016/j.jngse.2020.103582.
26. Wang, G.; Leus, K.; Jena, H.S.; Krishnaraj, C.; Zhao, S.; Depauw, H.; Tahir, N.; Liu, Y.-Y.; Van Der Voort, P. A fluorine-containing hydrophobic covalent triazine framework with excellent selective CO_2 capture performance. *J. Mater. Chem. A* **2018**, *6*, 6370-6375, doi:10.1039/C7TA08913A.
27. Zhao, Y.; Yao, K.X.; Teng, B.; Zhang, T.; Han, Y. A perfluorinated covalent triazine-based framework for highly selective and water–tolerant CO_2 capture. *Energy Environ. Sci.* **2013**, *6*, 3684-3692. doi:10.1039/C3EE42548G.
28. Dawson, R.; Cooper, A.I.; Adams, D.J. Chemical functionalization strategies for carbon dioxide capture in microporous organic polymers. *Polym. Int*. **2013**, *62*, 345-352. https://doi.org/10.1002/pi.4407.
29. Flaig, R.W.; Osborn Popp, T.M.; Fracaroli, A.M.; Kapustin, E.A.; Kalmutzki, M.J.; Altamimi, R.M.; Fathieh, F.; Reimer, J.A.; Yaghi, O.M. The Chemistry of CO_2 Capture in an Amine-Functionalized Metal–Organic Framework under Dry and Humid Conditions. *J. Am. Chem. Soc* **2017**, *139*, 12125-12128. doi:10.1021/jacs.7b06382.
30. Gunasekar, G.H.; Park, K.; Ganesan, V.; Lee, K.; Kim, N.-K.; Jung, K.-D.; Yoon, S. A Covalent Triazine Framework, Functionalized with Ir/N-Heterocyclic Carbene Sites, for the Efficient Hydrogenation of CO_2 to Formate. *Chem. Mater*. **2017**, *29*, 6740-6748. doi:10.1021/acs.chemmater.7b01539.
31. Jia, J.; Chen, Z.; Belmabkhout, Y.; Adil, K.; Bhatt, P.M.; Solovyeva, V.A.; Shekhah, O.; Eddaoudi, M. Carbonization of covalent triazine-based frameworks via ionic liquid induction. *J. Mater. Chem. A* **2018**, *6*, 15564-15568. doi:10.1039/C8TA05583A.
32. Keskin, S.; van Heest, T.M.; Sholl, D.S. Can Metal–Organic Framework Materials Play a Useful Role in Large-Scale Carbon Dioxide Separations? *ChemSusChem* **2010**, *3*, 879-891. https://doi.org/10.1002/cssc.201000114.
33. Zhang, Y.; Jin, S. Recent Advancements in the Synthesis of Covalent Triazine Frameworks for Energy and Environmental Applications. *Polym.J.* **2019**, *11*, doi:10.3390/polym11010031.
34. Zhang, L.; Li, X.; Antonietti, M. General, Metal-free Synthesis of Carbon Nanofiber Assemblies from Plant Oils. *Angew. Chem. Int. Ed*. **2021**, *60*, 24257-24265. https://doi.org/10.1002/anie.202110725.
35. Katekomol, P.; Roeser, J.; Bojdys, M.; Weber, J.; Thomas, A. Covalent Triazine Frameworks Prepared from 1,3,5-Tricyanobenzene. Chem. Mater. **2013**, *25*, 1542-1548. doi:10.1021/cm303751n.
36. Kuecken, S.; Schmidt, J.; Zhi, L.; Thomas, A. Conversion of amorphous polymer networks to covalent organic frameworks under ionothermal conditions: a facile synthesis route for covalent triazine frameworks. J. Mater. Chem. A **2015**, *3*, 24422-24427. doi:10.1039/C5TA07408H.
37. Bojdys, M.J.; Jeromenok, J.; Thomas, A.; Antonietti, M. Rational Extension of the Family of Layered, Covalent, Triazine-Based Frameworks with Regular Porosity. Adv. Mater. **2010**, *22(19)*, 2202-2205. Doi: 10.1002/adma.200903436.
38. Ren. S.; Bojdys, M.J.; Dawson, R.; Laybourn, A.; Khimyak, Y.Z.; Adams, D.J. Cooper, A.I. Porous, Fluorescent, Covalent Triazine-Based Frameworks Via Room-Temperature and Microwave-Assisted Synthesis. Adv. Mater. **2012**, *24*, 2357-2361. Doi: 10.1002/adma.201200751.
39. Bhunia, A.; Vasylyeva, V.; Janiak, C. From a Supramolecular Tetranitrile to a Porous Covalent Triazine-Based Framework with High Gas Uptake Capacities. *Chem. Commun.* **2013**, *49* (38), 3961. https://doi.org/10.1039/c3cc41382a.
40. Rademacher, L.; Beglau, T.H.Y.; Ali, B.; Sondermann, L.; Strothmann, T.; Boldog, I.; Barthel, J.; Janiak, C. Ruthenium nanoparticles on covalent triazine frameworks incorporating thiophene for the electrocatalytic hydrogen evolution reaction. *J. Mater. Chem. A* **2024**, *12*, 2093-2109. https://doi.org/10.1039/D3TA05597C.

 doi:10.20944/preprints202507.0335.v1

41. Rademacher, L.; Beglau, T.H.Y; Heinen, T.; Barthel, J.; Janiak, C. Microwave-assisted synthesis of iridium oxide and palladium nanoparticles supported on a nitrogen-rich covalent triazine framework as superior electrocatalysts for the hydrogen evolution and oxygen reduction reaction. *Front. Chem.* **2022**, *10*, 945261. https://doi.org/10.3389/fchem.2022.945261.
42. Öztürk, S.; Xiao, Y.-X.; Dietrich, D.; Giesen, B.; Barthel, J.; Ying, J.; Yang, X.-Y.; Janiak, C. Nickel nanoparticles supported on a covalent triazine framework as electrocatalyst for oxygen evolution reaction and oxygen reduction reactions. *Beilstein J. Nanotechnol.* **2020**, *11*, 770-781. https://doi.org/10.3762/bjnano.11.62.
43. Dey, S.; Bhunia, A.; Breitzke, H.; Groszewicz, P.B.; Buntkowsky, G.; Janiak, C. Two linkers are better than one: enhancing CO_2 capture and separation with porous covalent triazine-based frameworks from mixed nitrile linkers. *J. Mater. Chem. A* **2017**, *5*, 3609-3620. doi:10.1039/C6TA07076K.
44. Oxley, J.C.; Smith, J.L.; Moran, J.S. Decomposition of Azo- and Hydrazo-Linked Bis Triazines. *J. Energ. Mater* **2009**, *27*, 63-93. doi:10.1080/07370650802405174.
45. Kuhn, P.; Thomas, A.; Antonietti, M. Toward Tailorable Porous Organic Polymer Networks: A High-Temperature Dynamic Polymerization Scheme Based on Aromatic Nitriles. *Macromolecules* **2009**, *42*, 319-326. doi:10.1021/ma802322j.
46. Preis, E.; Dong, W.; Brunklaus, G.; Scherf, U. Microporous, tetraarylethylene-based polymer networks generated in a reductive polyolefination process. *Journal of Materials Chemistry C* **2015**, *3*, 1582-1587. doi:10.1039/C4TC02664K
47. Dey, S.; Bhunia, A.; Boldog, I.; Janiak, C. A mixed-linker approach towards improving covalent triazine-based frameworks for CO_2 capture and separation. *Microporous Mesoporous Mater.* **2017**, *241*, 303-315. https://doi.org/10.1016/j.micromeso.2016.11.033.
48. Bhunia, A.; Vasylyeva, V.; Janiak, C. From a supramolecular tetranitrile to a porous covalent triazine-based framework with high gas uptake capacities. *Chem. Commun.* **2013**, *49*, 3961-3963. doi:10.1039/C3CC41382A.
49. Bhunia, A.; Boldog, I.; Möller, A.; Janiak, C. Highly stable nanoporous covalent triazine-based frameworks with an adamantane core for carbon dioxide sorption and separation. *J.Mater.Chem.A* **2013**, *1*, 14990-14999. doi:10.1039/C3TA13407E.
50. Tao, L.; Niu, F.; Liu, J.; Wang, T.; Wang, Q. Troger's base functionalized covalent triazine frameworks for CO_2 capture. *RSC Advances* **2016**, *6*, 94365-94372, doi:10.1039/C6RA21196H.
51. Quantachrome Instruments (1900 Corporate Drive, Boynton Beach, FL 33426 USA, http://www.quantachrome.com) Powder Tech Note 35.
52. Lim, H.; Cha, M. C.; Chang, J. Y. Preparation of Microporous Polymers Based on 1,3,5-Triazine Units Showing High CO2 Adsorption Capacity. *Macromol. Chem. Phys.* **2012**, *213* (13), 1385-1390. DOI: https://doi.org/10.1002/macp.201200195.
53. Lu, Y.-C.; Yang, J.-P.; Yang, B.-T.; Chen, C.-C.; Lai, L.-L. Introduction of a spiro-linker in triazine-based polymers to enlarge void space and increase IPA adsorbing capacity to 164.7 mg/g at 1000 ppm. *Journal of the Taiwan Institute of Chemical Engineers* **2022**, *140*, 104531. DOI: https://doi.org/10.1016/j.jtice.2022.104531.
54. Wang, H.; Jiang, D.; Huang, D.; Zeng, G.; Xu, P.; Lai, C.; Chen, M.; Cheng, M.; Zhang, C.; Wang, Z. Covalent triazine frameworks for carbon dioxide capture. *J. Mater. Chem. A* **2019**, *7*, 22848-22870. doi:10.1039/C9TA06847C.
55. Ozdemir, J.; Mosleh, I.; Abolhassani, M.; Greenlee, L.F.; Beitle, R.R.; Beyzavi, M.H. Covalent Organic Frameworks for the Capture, Fixation, or Reduction of CO_2. *Front. Energy Res.* **2019**, *7*, 77. doi:10.3389/fenrg.2019.00077.
56. Ismail, M.; Bustam, M.A.; Kari, N.E.; Yeong, Y.F. Ideal Adsorbed Solution Theory (IAST) of Carbon Dioxide and Methane Adsorption Using Magnesium Gallate Metal-Organic Framework (Mg-gallate). *Molecules* **2023**, *28*, 3016-3033. doi:10.3390/molecules28073016.
57. Nuhnen, A.; Janiak, C. A practical guide to calculate the isosteric heat/enthalpy of adsorption via adsorption isotherms in metal–organic frameworks, MOFs. *Dalton Trans* **2020**, *49*, 10295-1030. doi:10.1039/D0DT01784A.

 doi:10.20944/preprints202507.0335.v1

58. Sánchez, M.I.; Martínez-Costas, J.; Mascareñas, J.L.; Vázquez, M.E. MitoBlue: A Nontoxic and Photostable Blue-Emitting Dye That Selectively Labels Functional Mitochondria. *ACS Chem. Biol* **2014**, *9*, 2742-2747. doi:10.1021/cb500552f.
59. Tuci, G.; Iemhoff, A.; Ba, H.; Luconi, L.; Rossin, A.; Papaefthimiou, V.; Palkovits, R.; Artz, J.; Pham-Huu, C.; Giambastiani, G. Playing with covalent triazine framework tiles for improved CO_2 adsorption properties and catalytic performance. *Beilstein J. Nanotechnol.* **2019**, *10*, 1217-1227. doi:10.3762/bjnano.10.121.
60. Tuci, G.; Pilaski, M.; Ba, H.; Rossin, A.; Luconi, L.; Caporali, S.; Pham-Huu, C.; Palkovits, R.; Giambastiani, G. Unraveling Surface Basicity and Bulk Morphology Relationship on Covalent Triazine Frameworks with Unique Catalytic and Gas Adsorption Properties. *Adv. Funct. Mater*. **2017**, *27*, 1605672. https://doi.org/10.1002/adfm.201605672.
61. Hug, S.; Stegbauer, L.; Oh, H.; Hirscher, M.; Lotsch, B.V. Nitrogen-Rich Covalent Triazine Frameworks as High-Performance Platforms for Selective Carbon Capture and Storage. *Chem. Mater*. **2015**, *27*, 8001-8010. doi:10.1021/acs.chemmater.5b03330.
62. Hug, S.; Mesch, M.B.; Oh, H.; Popp, N.; Hirscher, M.; Senker, J.; Lotsch, B.V. A fluorene based covalent triazine framework with high CO_2 and H_2 capture and storage capacities. *J. Mater. Chem. A* **2014**, *2*, 5928-5936. doi:10.1039/C3TA15417C.
63. Zhu, X.; Tian, C.; Veith, G.M.; Abney, C.W.; Dehaudt, J.; Dai, S. In Situ Doping Strategy for the Preparation of Conjugated Triazine Frameworks Displaying Efficient CO_2 Capture Performance. *J. Am. Chem. Soc*. **2016**, *138*, 11497-11500. doi:10.1021/jacs.6b07644.
64. Lee, Y.J.; Talapaneni, S.N.; Coskun, A. Chemically Activated Covalent Triazine Frameworks with Enhanced Textural Properties for High Capacity Gas Storage. *ACS Appl. Mater. Interfaces* **2017**, *9*, 30679-30685. doi:10.1021/acsami.7b08930.
65. Yuan, K.; Liu, C.; Zong, L.; Yu, G.; Cheng, S.; Wang, J.; Weng, Z.; Jian, X. Promoting and Tuning Porosity of Flexible Ether-Linked Phthalazinone-Based Covalent Triazine Frameworks Utilizing Substitution Effect for Effective CO_2 Capture. *ACS Appl. Mater. Interfaces* **2017**, *9*, 13201-13212. doi:10.1021/acsami.7b01783.
66. Wang, G.; Leus, K.; Zhao, S.; Van Der Voort, P. Newly Designed Covalent Triazine Framework Based on Novel N-Heteroaromatic Building Blocks for Efficient CO_2 and H_2 Capture and Storage. *ACS Appl. Mater. Interfaces* **2018**, *10*, 1244-1249. doi:10.1021/acsami.7b16239.
67. Park, K.; Lee, K.; Kim, H.; Ganesan, V.; Cho, K.; Jeong, S.K.; Yoon, S. Preparation of covalent triazine frameworks with imidazolium cations embedded in basic sites and their application for CO_2 capture. *J. Mater. Chem. A* **2017**, *5*, 8576-8582. doi:10.1039/C6TA11226A.
68. Fu, Y.; Wang, Z.; Li, S.; He, X.; Pan, C.; Yan, J.; Yu, G. Functionalized Covalent Triazine Frameworks for Effective CO_2 and SO_2 Removal. *ACS Appl. Mater. Interfaces* **2018**, *10*, 36002-36009. doi:10.1021/acsami.8b13417.
69. Yuan, K.; Liu, C.; Liu, C.; Zhang, S.; Yu, G.; Yang, L.; Yang, F.; Jian, X. Construction of triphenylamine functional phthalazinone-based covalent triazine frameworks for effective CO_2 capture. *Polym. J.* **2018**, *151*, 65-74. https://doi.org/10.1016/j.polymer.2018.07.061.
70. Du, J.; Liu, Y.; Krishna, R.; Yu, Y.; Cui, Y.; Wang, S.; Liu, Y.; Song, X.; Liang, Z. Enhancing Gas Sorption and Separation Performance via Bisbenzimidazole Functionalization of Highly Porous Covalent Triazine Frameworks. *ACS Appl. Mater. Interfaces* **2018**, *10*, 26678-26686. doi:10.1021/acsami.8b08625.
71. Jena, H.S.; Krishnaraj, C.; Wang, G.; Leus, K.; Schmidt, J.; Chaoui, N.; Van Der Voort, P. Acetylacetone Covalent Triazine Framework: An Efficient Carbon Capture and Storage Material and a Highly Stable Heterogeneous Catalyst. *Chem. Mater*. **2018,** *30*, 4102-4111. doi:10.1021/acs.chemmater.8b01409.
72. Mukherjee, S.; Das, M.; Manna, A.; Krishna, R.; Das, S. Newly designed 1,2,3-triazole functionalized covalent triazine frameworks with exceptionally high uptake capacity for both CO_2 and H_2. *J. Mater. Chem. A* **2019**, *7*, 1055-1068. doi:10.1039/C8TA08185A.